

# 13 Hindcast AGCM Experiments on the Predictability of Stratospheric Sudden Warming

Hitoshi Mukougawa<sup>1</sup>, Toshihiko Hirooka<sup>2</sup>, Tomoko Ichimaru<sup>3</sup> and Yuhji Kuroda<sup>4</sup>

<sup>1</sup> Kyoto University, Disaster Prevention Research Institute, mukou@dpac.dpri.kyoto-u.ac.jp

<sup>2</sup> Kyushu University, Department of Earth and Planetary Sciences, hirook@geo.kyushu-u.ac.jp

<sup>3</sup> Kyushu University, Department of Earth and Planetary Sciences, ichimaru@geo.kyushu-u.ac.jp

<sup>4</sup> Meteorological Research Institute, kuroda@mri-jma.go.jp

**Abstract.** High sensitivity to the initial condition of the prediction for a stratospheric sudden warming (SSW) event occurring in December 2001 reported by Mukougawa, Sakai, and Hirooka (2005) is confirmed by conducting a series of hindcast experiments using an atmospheric general circulation model (MRI/JMA-GCM). Similar precursory circulation anomaly in the troposphere for the occurrence of the SSW is also obtained through a regression analysis on the GCM experiments. Furthermore, it is revealed that the response of stratospheric circulation to the magnitude of the precursory anomaly is nonlinear, which suggests the existence of a threshold magnitude of the precursory anomaly for the occurrence of the SSW. Detailed investigation on the precursory event will enable us to reveal the dynamical relationship between tropospheric circulation anomaly and the subsequent SSW.

## 1 Introduction

Predictability studies on large-scale atmospheric motions have been mainly dealing with the tropospheric circulations (e.g., Kimoto, Mukougawa, and Yoden 1992), and interests on the predictability of the stratospheric motions are quite limited except for some pioneering works to simulate stratospheric sudden warming (SSW) events (e.g. Miyakoda, Strickler, and Hembree 1970; Mechoso, Yamazaki, Kitoh, and Arakawa 1985; Mechoso, Suarez, Yamazaki, Kitoh, and Arakawa 1986). SSWs are the most spectacular planetary-scale event in the wintertime stratospheric circulation. However, the predictability of the SSW has recently attracted much attention by upsurging interests on the downward influence of the stratospheric circulation change into the troposphere (Christiansen 2003; Reichler, Kushner, and Polvani 2005).

Mukougawa and Hirooka (2004) first reported prolonged predictability of a SSW event occurring in Dec 1998 up to 1 month by investigating 1-month forecasts issued once a week by the Japan Meteorological Agency (JMA). However, since their results were based upon control forecasts starting from initial conditions without any perturbation, the practical predictability of the SSW could not be assessed precisely. Then, Mukougawa, Sakai, and Hirooka (2005) (hereafter referred to as M05) examined

practical predictability of a SSW event occurring in Dec 2001 using all ensemble members of the JMA 1-month forecasts. They found that the SSW is predictable from at least 2 weeks in advance. Moreover, they revealed that the predictability of the SSW depends on the initial time of the forecast, and found the existence of high sensitivity to the initial condition for the SSW prediction during the onset period of the SSW. Similar variations of the predictability were also documented by Kimoto et al. (1992) for the forecast of a tropospheric blocking event.

The basic mechanism of SSW events has been already established by Matsuno (1971) in the framework of dynamical interactions between stratospheric zonal flows and upward propagating planetary waves from the troposphere. However, tropospheric precursors which generate and promote the upward propagation of planetary waves for the onset of the SSW have not been fully documented. The study of M05 detected a possible tropospheric precursor for the SSW event in Dec 2001 using a regression analysis for the JMA 1-month ensemble prediction. By this statistical analysis, they found that a characteristic zonal wind anomaly pattern in the upper troposphere associated with a persistent blocking event is significantly related to the subsequent occurrence of the SSW. However, since their work is based on a statistical analysis, we cannot confirm whether the statistically obtained precursor actually induces the following SSW.

Thus, in order to confirm the dynamical relevance of the obtained tropospheric precursor to the occurrence of the SSW event occurring in Dec 2001, we will conduct a series of hindcast experiments using an atmospheric general circulation model (MRI/JMA-GCM) in this study. The existence of high sensitivity to the initial condition for the SSW prediction reported by M05 will be also re-examined by the MRI/JMA-GCM experiments. We believe that detailed investigation on the precursory event by these hindcast experiments will enable us to reveal the dynamical relationship between tropospheric blocking event and the subsequent SSW.

## 2 Model

The model used in this study is a general circulation model (MRI/JMA-GCM) developed by the Japan Meteorological Agency (JMA) and Meteorological Research Institute (MRI) (Mizuta, Oouchi, Yoshimura, Noda, Katayama, Yukimoto, Hosaka, Kusunoki, Kawai, and Nakagawa 2006). The model is based on a global weather prediction model of the JMA (JMA-GSM0103), which was used to perform the JMA 1-month ensemble prediction during 2001/2002 winter. The 1-month forecast dataset was investigated in M05.

The computations were performed at a triangular truncation 96 with the linear Gaussian grid (TL96) in the horizontal. The model has 40 levels in the vertical, with the model top at 0.4 hPa. A semi-Lagrangian scheme is used to calculate the horizontal advection terms. The cumulus convection scheme proposed by Arakawa and Schubert (1974), and the level 2 turbulence closure scheme by Mellor and Yamada (1974) are implemented. Several physical processes important for the stratosphere, such as radiation, gravity wave drag, and a direct aerosol effect for the radiation processes are also implemented. The concentration of ozone is specified by the zonal-mean climatologi-

cal value during the computation. As boundary conditions, we used the monthly mean climatological sea surface temperature (SST) added with a constant SST anomaly from the climatology at the initial time. For further model details, the reader should consult JMA (2002) and Mizuta et al. (2006).

The initial conditions for the computations are identical to those used in M05, and are specified by the analysis added with initial perturbations in the JMA operational 1-month ensemble forecast. The JMA 1-month ensemble forecasts were conducted every Wednesday and Thursday from unperturbed initial condition and 12 perturbed conditions during 2001/2002 winter. The initial perturbations were obtained using the Breeding of Growing Modes (BGM) method (Toth and Kalnay 1993). They were applied to all pressure levels north of 20N with amplitude set to be 14.5 % of the climatological root-mean-square variance of 500-hPa heights. To verify model computations, JMA Global Analyses data set with 1.25-degree horizontal resolution at 23 levels from 1000 to 0.4 hPa is used.

### 3 Results

#### 3.1 High sensitivity to the initial condition

At first, we checked the reproduction of high sensitivity to the initial condition observed prior to the onset of SSW shown in M05. The thick solid lines in Fig. 13.1 show the daily time series of the observed 10-hPa zonal mean temperature ( $T$ ) at 80N. The temperature attains its peak on 28 Dec 2001. This warming is caused by the amplification of zonal wavenumber (WN) 1 planetary waves as seen in Fig. 13.2a which shows 3-day mean 10-hPa geopotential height during 27-29 Dec. The thin lines in Fig. 13.1 show the results of 30-day time integrations of MRI/JMA-GCM from initial conditions of the JMA ensemble 1-month forecasts starting from 5 and 6 Dec (Fig. 13.1a) and from 12 and 13 Dec (Fig. 13.1b). Some members successfully reproduce the occurrence of the SSW event for the computations from 5 and 6 Dec, while all the members starting from 12 and 13 well predict the warming episode as shown by M05. We also see that MRI/JMA-GCM tends to predict warmer temperatures in the polar stratospheric region for the SSW compared with the observation and the operational JMA 1-month forecasts (Fig. 13.1b). On the other hand, the forecasts starting from 5 and 6 Dec (Fig. 13.1a) have much larger spread among members than those from 12 and 13 Dec (Fig. 13.1b) during the mature phase of the SSW, in common with M05. Thus, we can also confirm high sensitivity to the initial condition for the prediction of the SSW during the onset period of the SSW by MRI/JMA-GCM hindcast experiments.

From Fig. 13.2, we can easily recognize a large spread among the ensemble members starting from 5 and 6 Dec. Figure 13.2b shows 3-day mean 10-hPa height field during 27-29 Dec for a forecast (run S) which attains the highest 10-hPa  $T$  at 80N on 28 Dec among the members, while Fig. 13.2c indicates a forecast (run F) with the lowest predicted temperature. For run S, the amplification of WN 1 component as for the analysis (Fig. 13.2a) is evident except for slight westward phase shift. For run F, however, the strong polar vortex still exists associated with low temperature in the

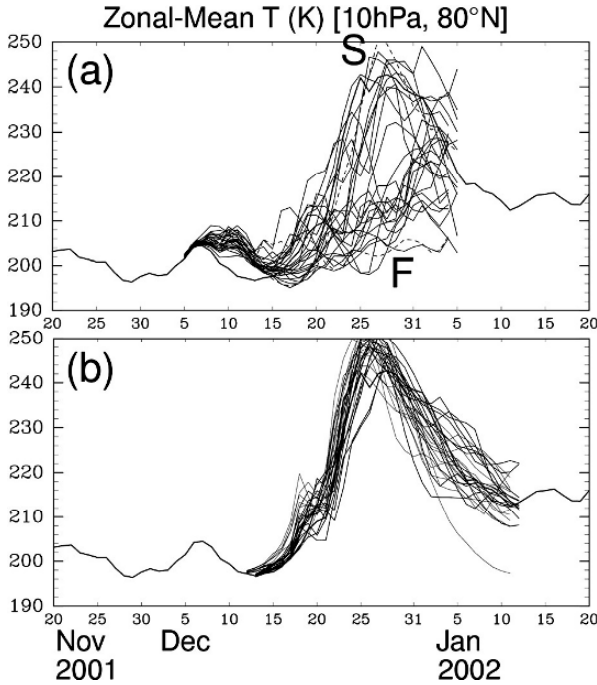


**Fig. 13.1.** Time variation of 10-hPa  $T$  at 80N from 20 Nov 2001 through 20 Jan 2002 for the analysis (thick solid lines), and for MRI/JMA GCM hindcast (thin solid lines) starting from 5 and 6 Dec 2001 (a), and 12 and 13 Dec 2001 (b). The dotted lines in (a) denote run S and run F.

polar region. Thus, the successful prediction for the amplification of WN 1 component is a key for the forecast of the SSW. As described in M05, the difference in the vertical component of WN 1 Eliassen-Palm (E-P) flux, which represents the vertical propagation of WN 1 wave activity (Andrews, Holton, and Leovy 1987), in higher latitudes of the lower stratosphere among ensemble members starting from 5 and 6 Dec becomes evident around 13 Dec. Therefore, we think that the period around Dec 13 corresponds to the onset of the SSW.

In order to find a necessary precursor for the SSW, we first compare the behavior of run S and run F during the onset period. Figure 13.3 shows 3-day mean 500-hPa geopotential height distributions for the onset period. The developed blocking high over the northeastern Atlantic shifts the Atlantic westerly jet considerably poleward in run S (Fig. 13.3b) as well as in the analysis (Fig. 13.3a). However, the blocking in run F (Fig. 13.3c) is much weaker, and the Atlantic jet resides near its climatological position around 60N. Since the blocking was already in a developing stage at the initial time of the hindcast experiment, weak persistence of the blocking is responsible for this difference. These features are also in common with those observed in M05.



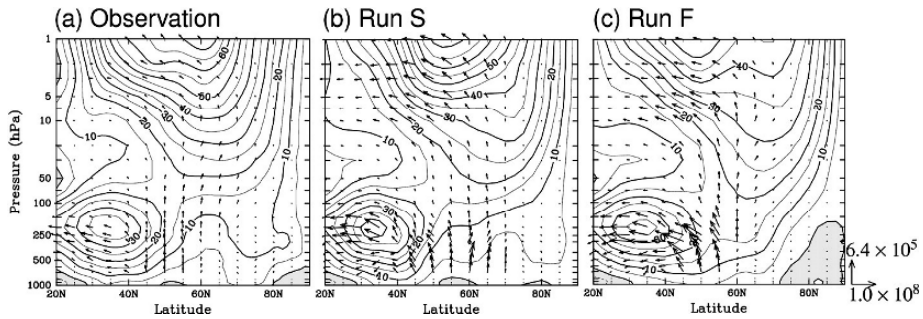


**Fig. 13.4.** Latitude-height cross sections of  $U$  (m/s) averaged over 12-14 Dec for the analysis (a), run S (b), and run F (c). The vectors show 3-day mean WN1 E-P flux ( $\text{kg/s}^2$ ) above 700 hPa. E-P flux is scaled by the reciprocal square root of the pressure. The magnitude of the reference vectors at 1000 hPa is shown in the lower right corner.

shown by E-P flux vectors in Fig. 13.4. Although run S and run F represent larger wave activity of WN 1 compared with the analysis, the poleward and upward propagation of WN 1 component in run S is much enhanced in the troposphere around 60N compared with run F. This might suggest the importance of WN 1 generation in the troposphere for the SSW prediction.

### 3.2 Regression analysis

The possible relationship between the blocking high over the northeastern Atlantic and the subsequent occurrence of the SSW as seen in Fig. 13.3 is also confirmed by the regression analysis of 500-hPa height field using all ensemble (26) members of the hindcast experiments starting from 5 and 6 Dec as in M05. Figure 13.5 shows 500-hPa height anomalies averaged over 12-14 Dec associated with a one-standard deviation anomaly of 10-hPa  $T$  on 28 Dec, corresponding to the warming peak. Here the anomaly is defined as the deviation from the ensemble mean of the hindcast experiments (Fig. 13.5b). Statistical significance of correlations is also assessed by Student's  $t$ -test based on 24 degrees of freedom, and shown by shades. The degree of freedom is deduced by considering that 26 ensemble members are independent each other. From this figure, we confirm that the positive height anomaly over the northeastern Atlantic associated with the blocking is well correlated with the subsequent occurrence of the SSW after 2 weeks, consistent with the previous analysis on run S and run F. The correlated height anomaly center over the Atlantic in Fig. 13.5 possess almost the same horizontal position as that in Fig. 3a in M05 while other significant anomalies seen in Fig. 13.5a have no corresponding anomalies in M05, which again suggests an important role of the blocking for the SSW.

The similar regression analysis for the computed 3-day mean  $U$  during 12-14 Dec against 10-hPa  $T$  on 28 Dec is shown in Fig. 13.6. From this figure, we also confirm that the upper-tropospheric  $U$  anomaly around 60N associated with the positive height anomaly is significantly correlated with the occurrence of the SSW, which is also observed in M05. However,  $U$  anomaly in subtropical regions (polar regions) of Fig. 13.6a is significant (insignificant), in contrast with Fig. 4a in M05. Figure 13.6a also

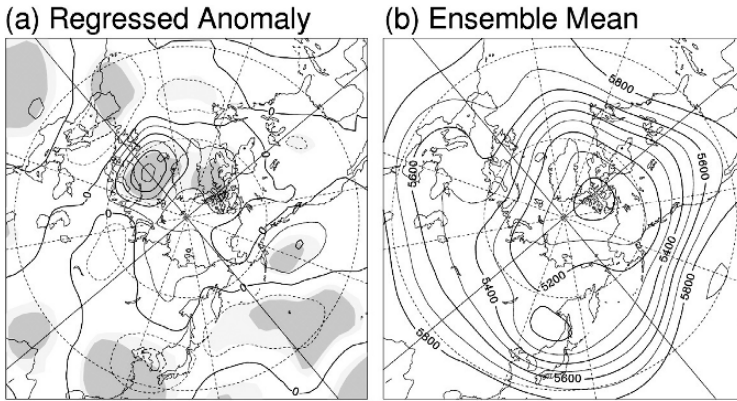


**Fig. 13.5.** (a) Regressed anomaly of the predicted 3-day mean 500-hPa height (m) during 12-14 Dec upon the predicted 10-hPa  $T$  at 80N on Dec 28 using all ensemble forecasts starting from 5 and 6 Dec by MRI-JMA GCM. The light (heavy) shades indicate regions where the statistical significance of the anomaly exceeds 95 (99)%. Contour interval is 20 m. (b) Ensemble average of the predicted 3-day mean 500-hPa height (m).

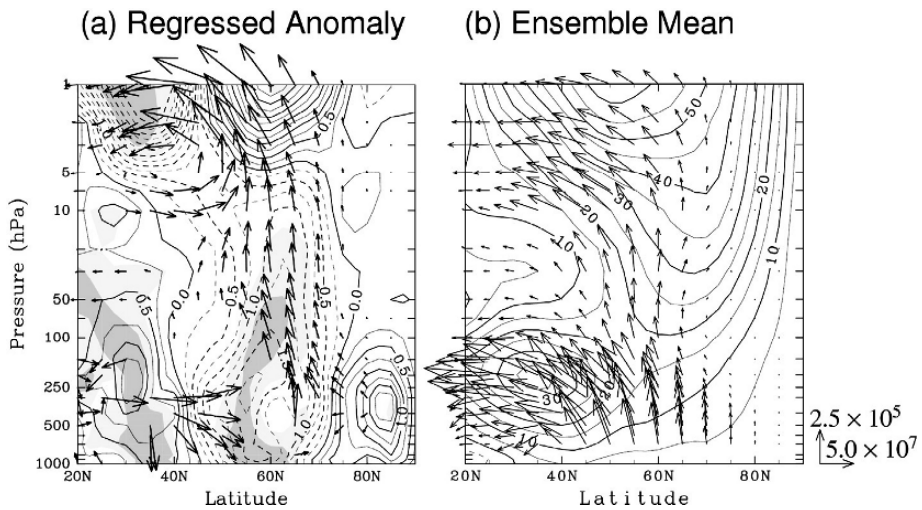


**Fig. 13.6.** As in Fig. 13.5, but for the predicted 3-day mean  $U$  (m/s) and WN 1 E-P flux ( $\text{kg/s}^2$ ) during 12-14 Dec. The vectors in (a) shows the regressed WN 1 E-P flux anomalies of which vertical or meridional component is significant at 90% level above 700 hPa. Their magnitude is multiplied by 10. E-P flux is scaled by the reciprocal square root of the pressure. The magnitude of the reference vectors at 1000 hPa is shown in the lower right corner.

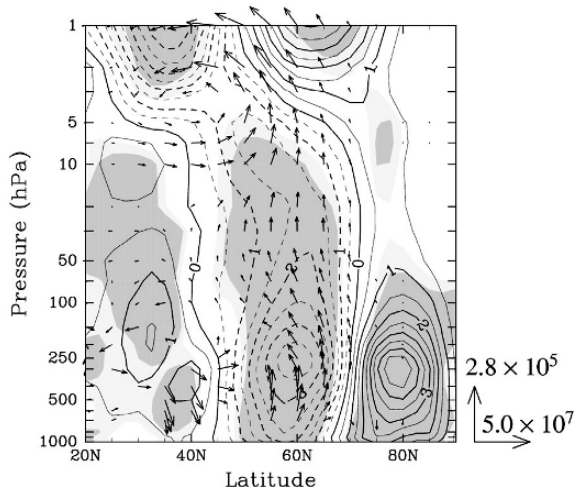
reveals that the poleward shift of upper stratospheric westerlies is also significantly correlated with the occurrence of the SSW as inferred from Fig. 13.4.

Figure 13.6a also shows the regressed anomaly of WN 1 E-P flux with statistical significance. Enhanced poleward propagation in the troposphere and active upward propagation from upper troposphere are intimately correlated with the SSW. The relationship is also in common with M05, but the statistical significance is much stronger compared with M05. Although the upward propagation of the ensemble averaged WN1 activity is most active around 60N in the lower stratosphere (Fig. 13.6b), the upward propagation is significantly enhanced around 70N. We also remark that the enhanced tropospheric generation of WN 1 component around 70N seems to be directly connected with the enhanced upward propagation to the stratosphere, which is not clearly seen in M05. These results would suggest that the generation rather than the propagation of WN 1 activity during the onset period is important for the occurrence of the SSW.

The high sensitivity to the initial condition for the SSW forecast found in Fig. 13.1a could be also inferred from Fig. 13.7 as in M05. This figure shows direction of the maximum spread among all ensemble members, represented by the regressed  $U$  anomalies on the leading principal component (PC1) of the computed 3-day mean  $U$  for 12-14 Dec of the hindcast experiments starting from 5 and 6 Dec. The EOF analysis was made for a domain from 1000 to 0.4 hPa poleward of 20N, and the data were weighted by the square root of the cosine of latitude as well as the square root of density at each level. The first EOF mode explains 43% of the total variance of  $U$  around the ensemble mean. The regressed  $U$  anomalies to PC1 have maxima in the upper troposphere, and are characterized by a barotropic tripole structure with nodes around 45N and 70N extending up to 10 hPa. In the upper stratosphere, a dipole structure of  $U$  anomaly with a node around 55N prevails. These features are very similar to the  $U$  profile correlated with the occurrence of the SSW shown in Fig. 13.6a. Thus, the coincidence could explain the reason why the high sensitivity to the initial condition is observed during the onset of the SSW as in M05. The regressed WN 1 E-P flux anomaly to PC1 as depicted by arrows in Fig. 13.7 also supports this conjecture. The upward propagation from the troposphere into the stratosphere around 60N is significantly enhanced as in Fig. 13.6a, which would trigger the SSW.

### 3.3 Hindcast Experiments using Regression Pattern

In order to reconfirm the important role of the statistically obtained regression pattern for the occurrence of the SSW shown in Figs. 13.5a and 13.6a, we performed a series of hindcast experiments starting from 13 Dec with several initial conditions composed of the ensemble mean field (Figs. 13.5b and 13.6b) and the regressed field multiplied by a coefficient  $\alpha$ . The ensemble as well as the regressed field was computed for all prognostic variables of MRI/JMA-GCM, using predicted 3-day mean values for 12-14 Dec based on the GCM ensemble experiments starting from 5 and 6 Dec.



**Fig. 13.7.** As in Fig. 13.6a, but for the regressed  $U$  and E-P flux vectors upon PC1 of the predicted 3-day mean  $U$  during 12-14 Dec of the ensemble forecasts starting from 5 and 6 Dec.

The hindcast experiments were conducted for a range of the coefficient  $\alpha$  from  $-2.0$  to  $4.0$  with an increment of  $0.5$ . The computation from the ensemble mean is given by  $\alpha = 0$ . We could expect from the regression analysis that positive  $\alpha$  will enhance the possibility for the occurrence of a SSW while negative  $\alpha$  will suppress SSW. The result of some hindcast experiments is shown by Fig. 13.8, which describes time evolution of the predicted  $T$  at 10 hPa and 80N. The numbers denoted on lines are  $\alpha$ . From this figure, we find that positively large  $\alpha$  actually tends to cause the warming while negatively large  $\alpha$  tends to suppress the warming around 28 Dec. Thus, the important role of the regressed pattern shown by Figs. 13.5a and 13.6a for the occurrence of the SSW is reconfirmed by the hindcast experiments using MRI/JMA-GCM.

The relationship between  $\alpha$  and predicted  $T$  at 10 hPa and 80N on 28 Dec is further examined by Fig. 13.9. The abscissa denotes  $\alpha$  and the ordinate  $T$  at 10 hPa and 80N on 28 Dec. Crosses are for the hindcast experiments starting from 13 Dec while open circles are for MRI/JMA-GCM ensemble experiments starting from 5 and 6 Dec, and the solid circle denotes the observation. The value of  $x$ -axis for each experiment and the observation is given by the projection coefficient of  $U(y,z)$  anomaly field  $\mathbf{a}$  onto the regressed field  $\mathbf{b}$  defined by  $\langle \mathbf{a}, \mathbf{b} \rangle / \langle \mathbf{b}, \mathbf{b} \rangle$ , where  $\langle \mathbf{a}, \mathbf{b} \rangle$  denotes the inner product between vectors  $\mathbf{a}$  and  $\mathbf{b}$  over the region of 20N-90N and 1000-0.4 hPa taking account of the areal factor proportional to cosine of latitude. The anomaly is defined by the difference of 3-day mean  $U$  during 12-14 Dec from the ensemble averaged field shown by Fig. 13.6b. It is noticeable from this figure that there is overall tendency of

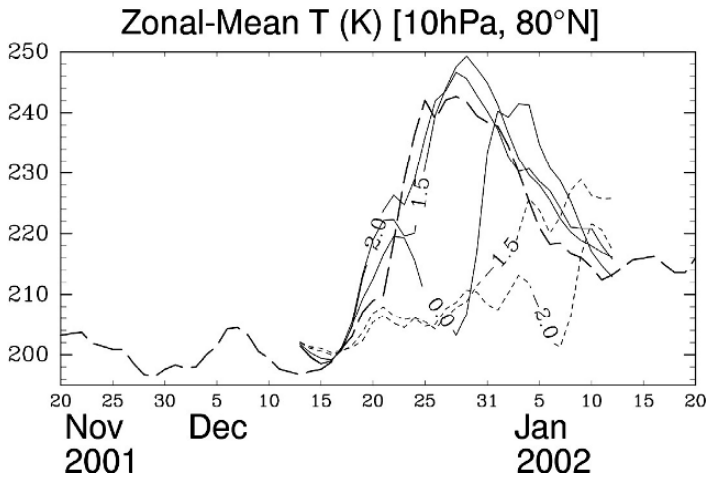


**Fig. 13.8.** As in Fig. 13.1, but for the MRI/JMA GCM hindcast experiments starting from 13 Dec 2001 with initial conditions composed of the ensemble mean field (Fig. 13.6b) and the regression field (Fig. 13.6a) multiplied by a coefficient  $\alpha$  which is denoted on the lines. The analysis is shown by the broken line, predictions with positive (negative) coefficients by thin solid (dotted) lines.

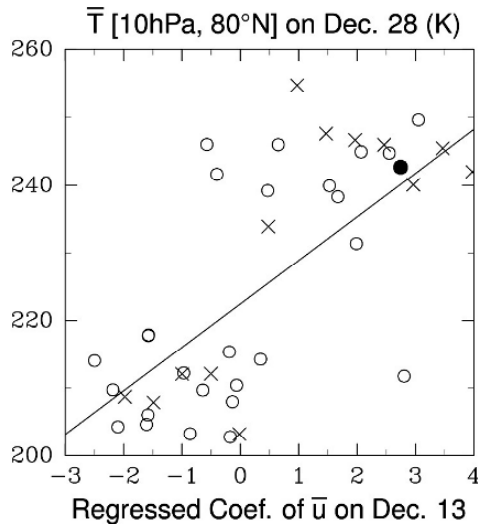


**Fig. 13.9.** Relationship between 10-hPa  $T$  (K) at 80N on Dec 28 and the coefficient  $\alpha$  of 3-day mean  $U$  anomaly during 12-14 Dec. Open circles are for ensemble experiments starting from 5 and 6 Dec, crosses are for hindcast experiments from 13 Dec starting from the ensemble mean field (Fig. 13.6b) added with the regression field (Fig. 13.6a) multiplied by the coefficient  $\alpha$  (value of the abscissa). The solid circle denotes the observation.

the increase of  $T$  on Dec. 28 with the increase of  $\alpha$ , which is shown by a regression line (solid line) in Fig. 13.9. However, the relationship is well described by a stepwise function of  $\alpha$  rather than a linear one. The computed  $T$  is clustered around 240 K (210 K) for positive (negative) values of  $\alpha$ . This also suggests the existence of a threshold value of  $\alpha$  for the occurrence of the SSW. Therefore, the stratospheric circulation responds nonlinearly to the magnitude of the precursory anomaly during the onset period of the SSW.

## 4 Concluding Remarks

Computations of MRI/JMA-GCM starting from the initial condition of each ensemble member for the JMA 1-month forecasts were performed to confirm the high sensitivity to the initial condition for the prediction of a WN 1 SSW event occurring in Dec 2001 reported by M05. The hindcast experiments well reproduced the similar high sensitivity to the initial condition during the onset period of the SSW.

The GCM experiments revealed that distinct  $U$  anomalies similar to those shown in M05 are significantly related to the subsequent warming in the stratospheric polar region. The characteristic tropospheric  $U$  anomalies were associated with persistent blocking over the Atlantic sector and enhanced upward propagation of WN 1 component from the troposphere into the stratosphere as in M05. Characteristic  $U$  anomalies in the stratosphere were also observed during the onset period of the SSW, which was not reported in M05. Moreover, generation of WN 1 component was much more distinct, and the statistical significance of tropospheric  $U$  anomalies was slightly reduced compared with M05. This difference suggests that the generation rather than the propagation of WN 1 is significantly related to the occurrence of the SSW. The pattern of  $U$  anomaly was also identified as the leading EOF pattern of  $U$  variations among ensemble members as in M05 during the onset period. Hence, the high sensitivity to the initial condition for the SSW prediction is connected with the coincidence between these two patterns.

The importance of the statistically obtained regressed field with respect to the subsequent SSW was also reconfirmed by conducting a series of hindcast experiments using MRI/JMA-GCM. The stratospheric warming tends to occur for initial conditions composed of ensemble mean field and the regressed field multiplied by positive coefficients although the magnitude of the warming does not linearly increase with increasing coefficient. Rather, the response is a stepwise function of the coefficient, which suggests the existence of a threshold value of the coefficient for the occurrence of the warming.

Such nonlinear feature of the stratospheric circulation reminds us the work of Yoden (1987). He showed the co-existence of two stable planetary flow regimes in the stratospheric circulation in a highly truncated atmospheric model for some parameter ranges. One corresponds to a strong polar vortex state with strong westerlies, and the other is similar to a SSW state with large-amplitude planetary waves. For such a nonlinear system, there must be a critical magnitude of initial perturbations to cause transitions from one stable state to the other across a “potential barrier” between two stable states. Moreover, there might be a preferred direction for the initial

perturbation to promote the transition at the “bifurcation point” where trajectories tend to diverge in a direction connecting these two stable states in phase space. The precursory anomalies for the SSW obtained through the regression analysis in this study would indicate such direction.

It would be possible to extract the most important ingredient for the occurrence of the SSW by conducting hindcast experiments from systematically idealized initial conditions produced from the regressed pattern. By these experiments, we could resolve the following interesting issues: the relevance of the tropospheric blocking to the subsequent SSW, the relative importance of the generation and propagation of planetary waves for the occurrence of the SSW, and the relationship between the generation of planetary waves and the tropospheric blocking. It is also very important to examine the predictability of other SSW events to reveal the robustness of the results obtained in this paper. Our preliminary analysis on the SSW event in January 2004 using JMA 1-month ensemble forecast dataset showed that the predictable period of the SSW event is at most 9 days, which is quite short compared with that of the SSW in December 2001. The SSW in December 2004 was significantly contributed by planetary wave components of smaller scales, i.e., WN 2 and 3. Therefore, it is necessary to conduct more detailed analysis to clarify the role of the smaller scale planetary waves on the predictability of the SSW events.

## Acknowledgments

We are grateful to H. Yoshimura for providing us MRI/JMA-GCM. We also would like to thank all the members in Climate Prediction Divisions in the JMA for providing us 1-month forecast data sets of the JMA. This work was supported by a Grant-in-Aid for Scientific Research (B) from JSPS, and by a Grant-in-Aid for the 21st Century COE Program (Kyoto University, G3). The GFD-DENNOU Library was used for the graphics.

## References

- Andrews, D. G., Holton, J. R. and Leovy, C. B. (1987) *Middle Atmosphere Dynamics*. Elsevier, New York.
- Arakawa, A. and Schubert, W. H. (1974) Interaction of cumulus cloud ensemble with the large-scale environment. Part I. *J. Atmos., Sci.*, 31, 674-701.
- Christiansen, B. (2003) Temporal growth and vertical propagation of perturbations in the winter atmosphere. *Q. J. R. Meteor. Soc.*, 129, 1589-1605.
- Japan Meteorological Agency (2002) Outline of the operational numerical weather prediction at the Japan Meteorological Agency (JMA). Appendix to *WMO Numerical Weather Prediction Progress Report*, JMA, Tokyo. pp. 157.
- Kimoto, M., Mukougawa, H. and Yoden, S. (1992) Medium-range forecast skill variation and blocking transition: A case study. *Mon. Wea. Rev.*, 120, 1616-1627.
- Matsuno, T. (1971) A dynamical model of stratospheric sudden warming. *J. Atmos., Sci.*, 27, 871-883.
- Mechoso, C. R., Yamazaki, K., Kitoh, A. and Arakawa, A. (1985) Numerical forecasts of stratospheric warming events during the winter of 1979. *Mon. Wea. Rev.*, 113, 1015-1029.

- Mechoso, C. R., Suarez, M. J., Yamazaki, K., Kitoh, A., and Arakawa, A. (1986) Numerical forecasts of tropospheric and stratospheric events during the winter of 1979: Sensitivity to the model's horizontal resolution and vertical extent. *Advances in Geophysics*, 29, 375-413.
- Mellor, G. L. and Yamada, T. (1974) A hierarchy of turbulence closure models for planetary boundary layers. *J. Atmos. Sci.*, 31, 1791-1806.
- Miyakoda, K., Strickler, R. F. and Hembree, G. D. (1970) Numerical simulation of the breakdown of a polar-night vortex in the stratosphere. *J. Atmos. Sci.*, 27, 139-154.
- Mizuta, R., Oouchi, K., Yoshimura, H., Noda, A., Katayama, K., Yukimoto, S., Hosaka, M., Kusunoki, S., Kawai, H. and Nakagawa M. (2006) 20-km-mech global climate simulations using JMA-GSM model. –Mean Climate States–. *J. Meteor. Soc. Japan*, 84, 165-185.
- Mukougawa, H. and Hirooka, T. (2004) Predictability of stratospheric sudden warming: A case study for 1998/99 winter. *Mon. Wea. Rev.*, 132, 1764-1776.
- Mukougawa, H., Sakai, H. and Hirooka, T. (2005) High sensitivity to the initial condition for the prediction of stratospheric sudden warming. *Geophys. Res. Lett.*, 32, L17806, doi:10.1029/2005GL022909.
- Reichler, T., Kushner, P. J. and Polvani, L. M. (2005) The coupled stratosphere-troposphere response to impulsive forcing from the troposphere. *J. Atmos. Sci.*, 62, 3337-3352.
- Toth, Z. and Kalnay, E. (1993) Ensemble forecasting at NMC; the generation of perturbations. *Bull. Am. Met. Soc.*, 74, 2317-2330.
- Yoden, S. (1987) Bifurcation properties of a stratospheric vacillation model. *J. Atmos. Sci.*, 44, 1723-1733.